3D Printed Fouling-resistant Composite Membranes

Saeed Mazinani, Abouther Al-Shimmery, Y.M. John Chew, Davide Mattia*

Department of Chemical Engineering, Centre for Advanced Separations Engineering,

University of Bath, Claverton Down, Bath BA2 7AY, UK

Corresponding author: y.m.chew@bath.ac.uk

ABSTRACT

Fouling remains a long-standing unsolved problem that hinders the widespread use of membrane applications in industry. This article reports the use of numerical simulations coupled with extensive materials synthesis and characterisation to fabricate fouling-resistant 3D printed composite membranes. The membranes consist of a thin polyethersulfone selective layer deposited onto a 3D printed flat and double sinusoidal (wavy) support. Fouling and cleaning of the composite membranes were tested by using bovine serum albumin (BSA) solution in a cross-flow ultrafiltration setup. The transmembrane pressure was regulated at 1 bar and the cross-flow Reynolds number (Re) varied between 400 and 1000. In comparison to the flat membrane, the wavy membrane showed superior performance in terms of pure water permeance (PWP) (10% higher) and permeance recovery ratio (87% versus 53%) after the first filtration cycle at Re = 1000. Prolong testing showed that the wavy membrane could retain approximately 87% of its initial PWP after 10 complete filtration cycles. This impressive fouling-resistant behaviour is attributed to the localised fluid turbulence induced by the 3D printed wavy structure. These results show that not only the lifetime of membrane operations could be favourably extended, but that the operational costs and environmental damage of membrane-based processes could also be significantly reduced.

Keywords: 3D printing; Bovine serum albumin; Polyethersulfone; Turbulence; Wavy composite membrane.

INTRODUCTION

Fouling is the accumulation of material on the surface or interior of a membrane and presents the largest challenge towards more widespread use of membranes in liquid separations, ranging from small scale operations, such as microfluidic devices, to large scale water treatment and waste recovery.[1] Fouling leads to flux decline, increased energy consumption, impaired quality of product and increased capital and operational costs associated with cleaning and replacement of worn-out membranes.[2] In a typical ultrafiltration (UF) unit, fouling can contribute up to 50% of the total operating costs.[3] To restore membrane performance, acidic and alkaline based cleaning agents are often employed to weaken or dissolve the fouling deposits.[4] Frequent use of these chemical agents not only poses significant health and environmental risks, but also affect the durability and integrity of the membranes.[5] As a consequence, there is intense interest in technology that can extend membrane performance *via* more sustainable fouling mitigation methods whilst reducing water, chemical and energy consumption.

A well-researched strategy to mitigate fouling is to modify the membranes' surface properties, either chemically or structurally.[5-6] Numerous approaches for the chemical modification of membrane surfaces have been widely tested, but all suffer from durability problems as once the membrane is fouled, the anti-fouling layer becomes ineffective.[7] Patterning of membrane surfaces,[8] on the other hand, is a promising chemical-free approach to promote fluid shear stress and create localised turbulence near the membrane surface, leading to reduced or slower fouling build-up.[9] A summary of relevant fouling and cleaning studies of patterned membranes and different types of fouling materials are summarised in Table S1[10-16]. Current patterning methods such as moulding, nanoimprinting and stamping suffer from insufficient fidelity and flexibility,[17] while at the same time negatively affecting the performance and durability of the membranes.[11] 3D printing, or additive manufacturing, can overcome these challenges by enabling the fabrication of complex/irregular patterns which would otherwise be impossible to manufacture using current techniques.[18]

Multi-jet printing (MJP) is one of the most versatile 3D fabrication processes due to its capability to produce complex yet detailed parts with high resolution.[19] A wide range of polymeric materials with various physical and mechanical properties ranging from rubber-like flexibility to ABS-like rigidity can be printed.[20] In the MJP fabrication process, tiny droplets of a UV-curable liquid resin are jetted onto a platform in the shape of the first layer by using a print-head and then immediately cross-linked by UV light to harden the shape of the layer. The building platform then steps down (by one layer thickness) and more material is deposited on top of the previous layer. This process continues layer by layer until the part is complete. During the fabrication process, the 3D printer uses a separate support material, i.e. hydroxylated wax, that allows the delicate features and complex internal cavities to be thoroughly cleaned without damage.[19, 21]

Despite this great potential, there are still very few studies that have used 3D printing for the fabrication of patterned membranes. These include the patterned anion exchange membranes fabricated *via* direct curing of photo-curable diurethane dimethacrylate by using a photolithographic process;[22] a 3D printed PDMS contactor, showing higher mass transfer compared to hollow fibre membranes;[23] 3D printed composite membranes generated by coating a polyethylene glycol (PEG) layer over a commercial UF membrane;[24] and patterned thin film composite membranes fabricated by a combination of ink-jet printing and interfacial polymerization, with the membrane exhibiting NaCl rejection performance similar to that of a commercial membrane.[25] More recently, a 3D composite membrane used to enhance the separation of oil/water mixtures was manufactured by depositing a PES selective layer on top of a 3D printed support with a wavy pattern.[26]

This study presents an innovative and systematic approach to design and fabricate fouling-resistant composite membranes by using a combination of computational modelling and 3D printing technology. Computational fluid dynamics (CFD) simulations coupled with extensive materials synthesis and characterisation were used to identify a set of optimal design parameters for the fabrication of 3D printed composite membranes with patterns that minimise the build-up of a common particulate-based biological foulant, bovine serum albumin (BSA). CFD simulations were first carried

out to identify the effect of the wavy pattern characteristics, namely the peak amplitude and wavelength, on the hydrodynamic profile of the feed solution. Membrane supports with different peak amplitudes and wavelengths were then printed by using an industrial Multi-jet 3D printer and UV-curable polyurethane acrylate oligomers (ABS-like plastics). Ultrafiltration thin PES selective layers were subsequently deposited onto these supports by vacuum filtration and the stability of the composite membranes were evaluated. The wavy 3D composite membranes were tested for multiple fouling and cleaning cycles in a cross-flow filtration setup and the results were compared in terms of permeance, rejection and fouling resistance with a flat 3D composite membrane as a reference.

MATERIALS AND METHODS

Materials

The membrane supports were fabricated by using non-porous urethane acrylate oligomers (acrylonitrile butadiene styrene (ABS)) and proprietary hydroxylated wax (*VisiJet® S300, 3D Systems*, USA) in a MJP 3D printer (*ProJet 3500 HD Max printer, 3D Systems*, USA). Polyethersulfone (PES, Ultrason, M_w = 55 kDa, *BASF*), as main polymer, polyethylene glycol (PEG, M_w = 400 g mol^{-1}, *Sigma*), as pore former, and dimethyl sulfoxide (DMSO, purity > 99%, *Sigma,* 80 g), as solvent, were used to prepare the dope solution for the selective layer. Phosphate buffer saline (PBS, pH = 7.4, *Sigma*) tablets, deionized water (DI, Veolia purification system, resistivity = 18.2 MΩ) were used for the preparation of PBS solutions. Commercial EZ Rinse-C oil (*3D Systems*, USA) was used for removing the wax from the pores of the printed membrane supports. Bovine serum albumin (BSA, 1 g L^{-1}, M_w = 67 kDa, pH = 7.0, heat shock fraction grade, purity > 98 %, *Sigma*) was used as the model foulant. Cyclohexane (99 %, *VWR*), n-Hexane (98.5 %, *VWR*), acetone (99 %, *Sigma*), isopropanol (99.5 %, *VWR*) and ethanol (99 %, *VWR*) were used in the chemical compatibility test.

Preparation of feed solutions

PBS solutions (pH = 7.4, 1 L) were prepared by dissolving PBS tablets (5 tablets) in deionized water (1 L). BSA feed solution of 1 g L^{-1} (pH = 7.35, 1 L) was prepared by dissolving BSA (1 g) in the PBS solution (1 L). Dissolution of BSA was aided by vigorous stirring by using a magnetic stirrer for at least 5 hours. Prior to running the fouling experiments, the freshly prepared feed solution was filtered with a filter paper (5 µm) to remove aggregated BSA.

Fabrication of the 3D composite membranes

There were three main steps to fabricate the 3D printed composite membrane: (i) printing of the 3D supports, (ii) preparation of selective layer by non-induced phase separation and (iii) deposition of selective layer over the support (Figure 1). A detailed procedure for the fabrication of 3D printed composite membrane has been reported in a previous publication.[26] Prior to each experiment, the composite membrane was immersed in deionized water for 6 hours. There was no delamination observed before and after all fouling and cleaning experiments.

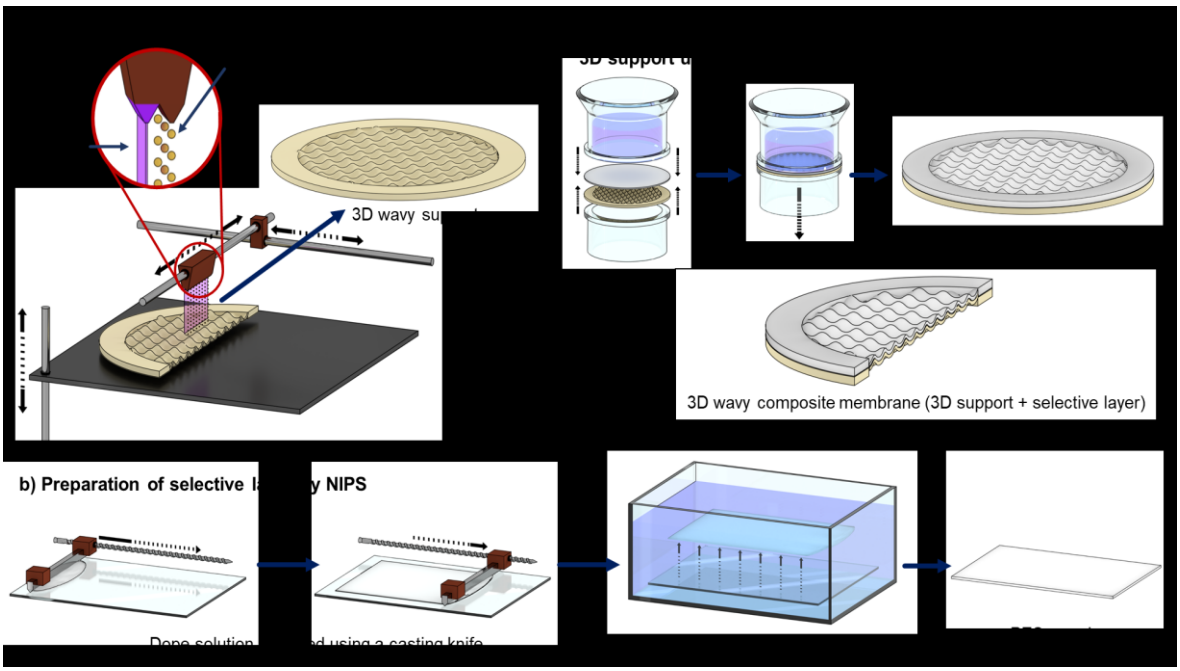

Figure 1. Preparation of wavy 3D composite membranes: (a) 3D printing of the wavy support; (b) casting of the PES selective layer; (c) vacuum filtration is used ensure adhesion of the selective layer onto the wavy support.

3D printing of the membrane supports

The porous area of the circular support was first designed with the Autodesk Inventor Professional (*2016 Inventor*, USA) program which enabled precision design of the desired pore sizes, distance between pores and number of pores. The OpenScad software was then used to design the wavy structure ($f(x,y) = 0.5 \times \sin(x) \times \sin(y)$) with the optimal peak amplitude and wavelength. Lastly, the pore structure was superimposed onto the wavy surface (37 mm diameter) and an edge/ring of 6.5 mm width was added to the porous area to give a total diameter of 50 mm. The CAD file was subsequently converted into stereolithography (STL) format and uploaded to the 3D printer. The same procedure was also used to prepare flat 3D supports. The effective filtration areas for the flat and wavy supports are 10.74 cm^2 and 12.16 cm^2, respectively, whilst both having the same footprint.

After the printing process was finished, the wax was removed from the pores. 50 ml of different solvents including hexane, cyclohexane, acetone, ethanol, warm soapy water and a commercial EZ Rinse-C oil were used to dissolve the wax material. Chemical compatibility experiments were conducted to determine the suitability of the solvents by measuring the change in mass of samples before and after immersing in the solvents. The printed supports (approximately 2.85 g) were submerged in individual chemicals for 3 hrs at room temperature. Then, they were dried for 1 hr and weighed with a balance. The mass change (%) of each piece was calculated. The 3D wavy supports were post-processed by ultra-sonication in the chemicals for 6 hrs at 60 ºC. The intrinsic permeability of each membrane support was measured by using the protocol reported by Chew *et al*.[27]

Preparation of PES selective layer and composite membrane

The PES selective layer was prepared by using non-induced phase separation (NIPS). Prior to use, the PES was dried in an oven at 60 ºC for 24 hrs. The dope solution was prepared by dissolving PES and PEG in Dimethyl sulfoxide (DMSO) at room temperature. DMSO was the preferred solvent because it is more environmentally friendly compared to other common solvents used for membrane fabrication such as N-Methyl-2-pyrrolidone (NMP), Dimethylacetamide (DMAc) and

Dimethylformamide (DMF).[28] The dope solution was casted uniformly on a glass plate using a casting knife with 100 μm gap height at room temperature (15-20 ºC) with approximately 25 % relative humidity. The nascent polymer films were exposed to air for 20 seconds to allow the solvent to evaporate. Thereafter, the films were immersed in the non-solvent water bath. To remove any traces of DMSO from the membrane films, they were kept in water for 2 days and the water in the bath was replaced with fresh water every 24 hours.

Numerical simulations

The conservation of mass and momentum equations, and particle tracing model for steady state and laminar flow conditions were solved by using a commercial CFD software COMSOL Multiphysics™ v5.4 to elucidate the fluid mechanics of the filtration process of flat and wavy 3D composite membranes. The flowing fluid was assumed to be Newtonian and incompressible in all the numerical models presented in this study. The governing equations and boundary conditions can be found in the supporting information.

Past experience[29] and separate simulations showed that full three-dimensional representation of the cross-flow filtration cell is unnecessary for this case as the wavy pattern of the membrane is regular and this will increase computing resources and time significantly (in the order of days) with marginal additional benefits to the purpose of this study. A comparison of the shear stress values predicted by using two- and three-dimensional representations is shown later in the Results and Discussion. The figure confirmed that the difference in the predicted shear stress values is negligible. Therefore, the authors decided to use two-dimensional simulation domains to represent the cross-section at the mid-point of the filtration cell, as shown in Figure 2. The overall domain size was 4 mm × 50 mm (height × length). The wavy pattern was set at $\alpha = 0.5$ mm, $f = 2$ s^{-1} and $\lambda = 3$ mm. The length of the active membrane surface (L), was 37 mm. The wavy and flat domains were discretised into 14250 and 12383 unstructured triangular elements, respectively, using finite element method.

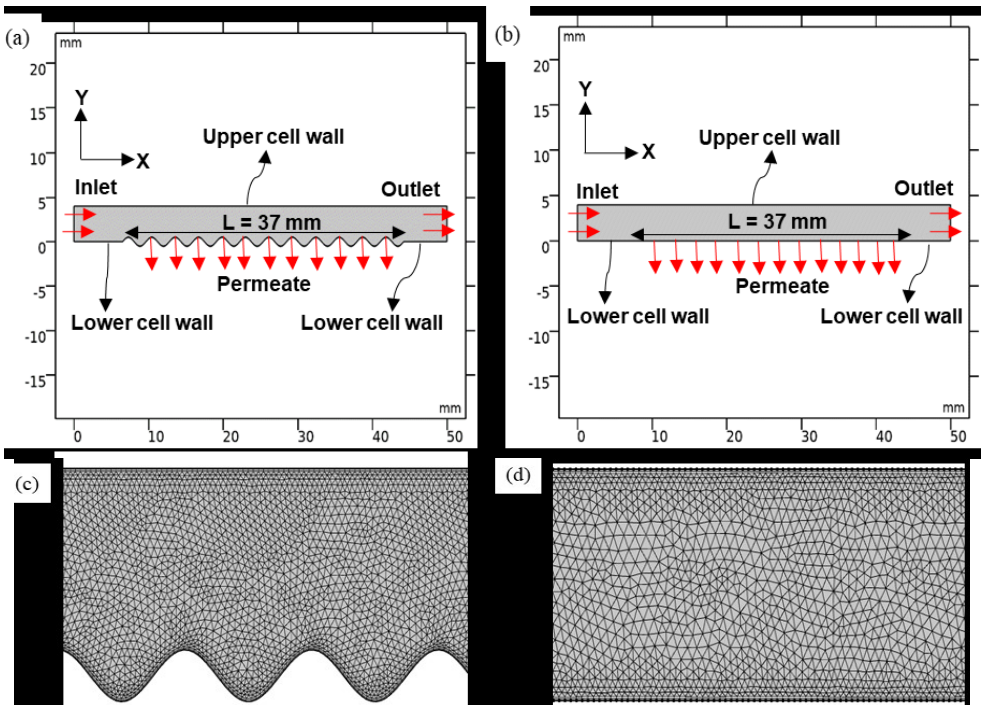

Figure 2. The geometry for (a) wavy and (b) flat membranes along with mesh discretisations for (c) wavy and (d) flat used in the simulations, with dimensions matching the cross-section at the mid-point of the filtration cell. A denser mesh was applied to the membrane surface and upper wall region where the velocity gradients were expected to vary more rapidly.

Characterisation of composite membrane

Morphology and wetting behaviour

The morphological characteristics of the membrane support, selective layer and 3D composite membrane were analysed using a scanning electron microscope (*JEOL FESEM6301F*) and a digital microscope (*VHX - 6000*, Japan). The surface roughness of the 3D support and selective layer was determined using atomic force microscopy (AFM; Nanosurf EasyScan 2 Flex, Switzerland) under ambient conditions in the tapping mode (scan size of 5 µm, time/line of 1 s, samples/line of 256) with a monolithic silicon AFM probe (Tap190Al-G, nominal tip radius: < 10 nm).

The porosity (%) of the composite membrane were determined based on the protocol reported by Zhang *et al.*[30] The nominal porosity of the membrane support was calculated using following equation:

$$Nominal\ porosity\ (\%) = \left(\frac{void\ volume}{total\ volume}\right)$$

$$= \left(\frac{n\ \times\ surface\ area\ of\ each\ pore}{total\ surface\ area\ of\ the\ support}\right) \qquad (1)$$

where n is the total number of pores. The actual porosity (number of open pores) of the membrane support was determined by comparing the mass difference between supports with and without pores:

$$Mass\ change = \left(1 - \frac{M_2}{M_1}\right) \times 100 \qquad (2)$$

where M_1 is the mass of membrane support without pores (kg) and M_2 is the mass of the support with pores (kg).

The wetting behaviour of the supports, selective layer and composite membranes was determined by measuring the water contact angles using a contact angle goniometer (*OCA machine, Data Physics*, Germany) at room temperature, using 5 µl droplets. The average of three measurements was reported.

Molecular weight cut-off (MWCO)

The molecular weight cut-off (MWCO) of the selective layer and composite membrane were determined by conducting solute rejection experiments in a dead-end cell using PEG solutions with molecular weights of 1000, 3000, 4000 and 6000 kDa. The authors adopted the protocol reported by Xu *et al.*[31] The concentration of PEG in respective feed solutions was analysed using a HPLC unit (1260 infinity series, Agilent Corporation, USA) consisting of an auto-sampler (G1329B) coupled with an evaporative light scattering detector (ELSD).

Filtration and anti-fouling performance

The filtration performance of the membranes was evaluated by using a circulating cross-flow apparatus (Figure S1). Prior to the filtration experiments, the membranes were pre-compacted using pure water at 2 bar until steady permeance was reached. The required duration for pre-compaction was just less than 2 hrs. The permeance, K, (LMH bar^{-1}) of the membrane was calculated by using equation (10):

$$K = \frac{V}{\Delta t \times A \times \Delta p} \tag{3}$$

where V is the volume of permeate collected (m^3) over time Δt (hr); A is the effective membrane area (m^2) for the flat and wavy membranes; The effective filtration areas for the flat and wavy supports were 10.74 and 12.16 cm^2, respectively, Δp is the transmembrane pressure (bar). All filtration experiments were carried out at 1 bar constant pressure and repeated three times. The BSA rejection of the composite membranes was calculated as follow:

$$R\ (\%) = \frac{C_F - C_P}{C_F} \tag{4}$$

where C_F is the BSA concentration in the feed solution (mg L^{-1}) and C_P is the BSA concentration on the permeate side (mg L^{-1}). The BSA concentrations of both feed and permeate were determined using a UV-Vis spectrophotometer (Cary, Agilent, USA) at a wave length of 278 nm. The average of three measurements was reported.

To evaluate the fouling-resistant property of the membranes, four fouling indices, permeance recovery ratio (PRR_i), reversible permeance decline ratio (RPR_i), irreversible permeance decline ratio ($IrPR_i$) and total permeance decline ratio (PDR_i), were calculated for each cycle as follows:[26]

$$PRR_i\ (\%) = \left(\frac{P_{W,i+1}}{P_{W,i}}\right) \times 100 \tag{5}$$

$$RPR_i(\%) = \left(\frac{P_{W,i+1} - P_{E,i}}{P_{W,i}}\right) \times 100 \tag{6}$$

$$IrPR_i(\%) = \left(\frac{P_{W,i} - P_{W,i+1}}{P_{W,i}}\right) \times 100 \quad (7)$$

$$PDR_i(\%) = \left(\frac{P_{W,i} - P_{E,i}}{P_{W,i}}\right) \times 100 \quad (8)$$

where i is the cycle number. Every fouling and cleaning experiment was initiated by measuring the pure water permeance for 30 minutes. Then, fouling was started by switching the feed stream to a continuously stirred tank containing 500 mL of fresh BSA (1 g L^{-1}) solution. The membrane was subjected to filtration of the BSA solution for 1 hr until the permeance ($P_{E,i}$) reached steady state. During the cleaning process, the feed was switched to a cleaning tank where the system was flushed with deionized water at the same feed flow rate for 15 minutes. After cleaning, the pure water permeance ($P_{W,i+1}$) was measured again for 30 minutes. This was followed by a new fouling cycle where 500 mL of fresh BSA solution was used to ensure similar operating conditions in each cycle. In this work, three cycles of filtration experimentation were carried out for each composite membrane. Ten (10) cycles of filtration experimentation were carried out one time for wavy 3D composite membrane.

RESULTS AND DISCUSSION

3D Printed Composite Membranes

Design and optimisation of membrane morphology

The fabrication of the more complex wavy support and its selective layer (Figure 3a-b) required careful considerations which include the resolution and accuracy of the 3D printer, the ability of the selective layer to form a conformal coating onto the wavy support, and the ideal hydrodynamic conditions that would minimise the build-up of BSA fouling. A multi-stage optimisation process was carried out by using CFD simulation and materials characterisation techniques to identify the optimal peak amplitude, α, and wavelength, λ of the wavy structure. First, the printable range of peak amplitude (0 mm < α < 1.50 mm) and wavelength (0 mm < λ < 12 mm) for the 3D printer used in this

work were identified experimentally. Second, the hydrodynamic profiles of the feed solution generated by the wavy structure were summarised in a contour plot of maximum achievable surface shear stress in Figure 3c. The localised flow patterns around the membrane surface were also examined to identify any primary and/or secondary flow recirculation. Examples of the flow pattern in the valleys of the wavy structure for the top and bottom range of α and λ are shown in Figures 3d-g. In general, higher shear stress and localised turbulence near the membrane surface are favourable to reduce adhesion of foulants and enhance cleaning in cross-flow configurations.[32] The lowest surface shear stress value of 0.26 Pa was predicted for a flat membrane, i.e. when $\alpha = \lambda = 0$, as expected. There are also no recirculation zones for the flat membrane.

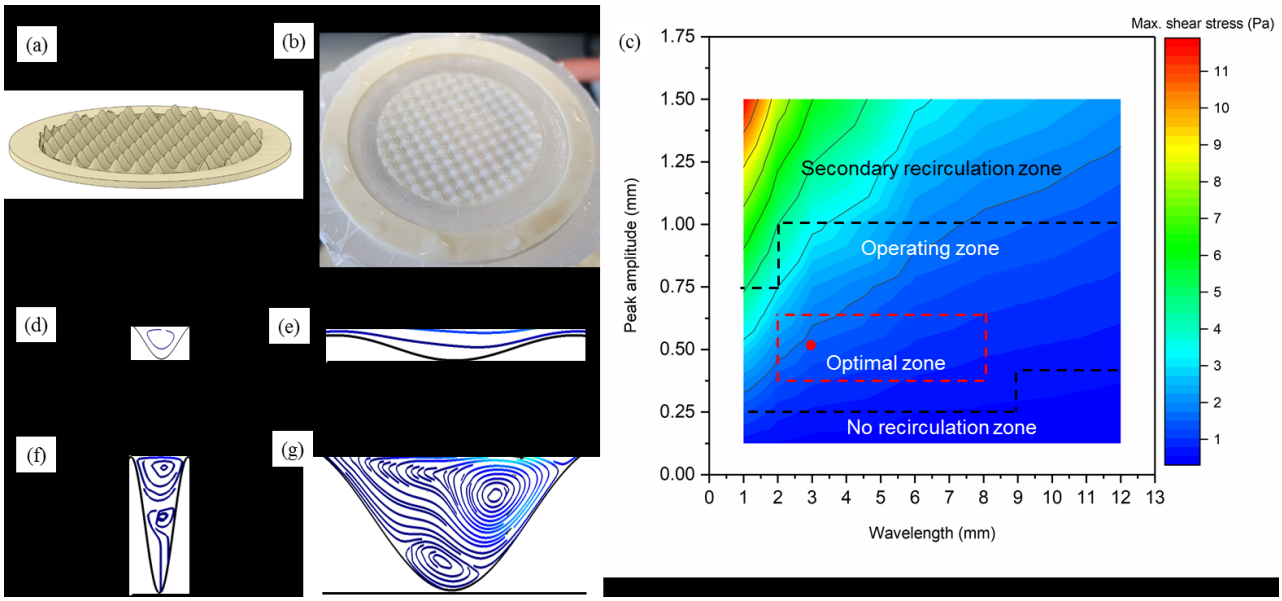

Figure 3. (a) Design of wavy support with nominal pores size and inter-pore spacing of 200 μm, amplitude, α = 1.50 mm and wavelength, λ = 3 mm; (b) conformal adhesion of PES selective layer onto the 3D printed wavy support; (c) contour plot of maximum surface shear stress for printable values of α and λ at cross-flow Re = 1000. Red: high shear stress and blue: low shear stress. The no recirculation, secondary recirculation, operating and optimal zones were divided by the dashed lines; flow patterns in the valley showing (d) no/limited flow recirculation for small α and short λ; (e) no/limited flow recirculation for low α and long λ; (f) secondary recirculation for large α and short λ; and (g) secondary recirculation for large α and long λ.

The contour plot of maximum achievable surface shear stress in Figure 3c can be divided into different zones:

No recirculation zone

When the peak amplitude is small *ca.* $0 < \alpha < 0.25$ mm, no sustained localised recirculation could form for all values of wavelength tested, $1 < \lambda < 12$ mm. This would result in low shear stress and, hence, limited ability to mitigate fouling due to turbulence. This region is called the 'no recirculation zone'.

Secondary recirculation zone

When the peak amplitude is large *ca.* $1.00 < \alpha < 1.50$ mm, large shear stress could be generated on the membrane surface for all values of wavelength tested and this is desirable for fouling mitigation. However, closer inspection of the flow pattern reveals the presence of secondary recirculation. Figures 3f-g show that areas of smaller recirculation form between the membrane surface and the primary recirculation area. This increases the possibility of fouling materials being trapped in these secondary areas, accumulating in the membrane valleys. This region is termed the 'secondary recirculation zone'.

Operating zone

The intermediate values of peak amplitude *ca.* $0.25 < \alpha < 1.00$ mm provide the preferred high surface shear stress condition with primary flow recirculation all values of wavelength tested. The magnitude of the surface shear stress in this 'operating zone' is also in the higher end of the spectrum of values employed in many cleaning-in-place industrial processes, e.g. in the dairy industry shear stress values used are between 2 and 6 Pa.[33]

Optimal zone

Within the operating zone, defined solely on the basis of hydrodynamic considerations, further restrictions on the values of peak amplitude and wavelength arise from materials considerations. For large α values within the operating zone, the selective layer would be pierced and the support would not be fully covered, whereas for long λ values, there was poor adhesion between the selective layer

and the wavy support. These limitations define the 'optimal zone' (*ca.* $0.38 < \alpha < 0.63$ mm and $2 < \lambda < 8$ mm) for the given combination of 3D printer used, materials and hydrodynamics. Ultimately, values of $\alpha = 0.5$ mm and $\lambda = 3$ mm were selected to ensure maximum shear stress (represented by the red dot in Figure 3c).

Fabrication of membrane support

The building material for the membrane support was a UV-cured polyurethane acrylate oligomer with the commercial name *VisiJet M3-X*. This ABS-like thermoplastic material has a high tensile strength and resistance to temperature along with good durability and stability which make it suitable being a membrane support.[34] The support material was hydroxylated wax with the commercial name *VisiJet S300*. This wax material offers hands-free, melt-away removal from inaccessible geometry features and internal spaces with no damage to the most delicate part features.[34] The removal of the hydroxylated wax proved challenging, given the very large number of small pores in the membrane support. A number of solvents were tested and assessed based on their ability to effectively remove the wax without damaging or swelling the membrane support. The experimental results of chemical compatibility and intrinsic permeability of the 3D supports are presented in the supporting information in Figure S2 and Table S2.

The mass change of the membrane supports after washing with *n*-hexane, cyclohexane, commercial EZ Rinse-C oil and warm water was negligible whereas deformation of the support was observed when acetone, isopropanol and ethanol were used. Amongst the chemically compatible solvents, the commercial EZ Rinse-C oil was selected as it provides the highest intrinsic membrane permeability, indicating that it could dissolve the largest amount of wax. Moreover, the commercial oil is more environmentally friendly compared to *n*-hexane and cyclohexane. Hence, the wax material for all the membrane supports in this study was removed by ultra-sonication in commercial EZ Rinse-C oil for 6 hrs at 60 ^{o}C.

Table 1 summarises the properties of wavy membrane supports with specified nominal pore diameter from 120 μm to 200 μm. The actual porosity and size of the pores on the membrane supports were determined *via* statistical image analysis of scanning electron microscopy (SEM) micrographs by analyzing more than 100 pores from randomly selected locations of the support by using *Image J*, and the average value recorded. A typical SEM micrograph for a wavy support with nominal pore size and inter-pore space of 200 μm is shown in Figure 4a.

The pore size distribution of the randomly selected pores is illustrated in Figure 4b. Although the nominal resolution of the 3D printer is 16 μm (layer thickness), experimentation with different combinations of nominal pore and inter-pore spacing values in the CAD design showed that larger values of both were required to obtain a higher proportion of open pores with a narrow pore size distribution once printed. It is also worth noting that nominal pore size and inter-pore spacing beyond 200 μm were also printed but full surface coverage of the selective layer could not be achieved because the selective layer was sucked into the larger pores during the vacuum coating process. Therefore, a nominal pore size of 200 μm and inter-pore spacing of 200 μm were selected for printing the membrane supports, since this combination results in the highest actual porosity, 14%, and intrinsic permeability 6×10^{-12} m^2.

Table 1. Summary of average pore size, porosity and intrinsic permeability of wavy supports with amplitude, $\alpha = 0.50$ mm and wavelength, $\lambda = 3$ mm.

Nominal pore size (μm)	Actual pore size (μm)	Number of pores	Number of open pores	Nominal porosity (%)	Actual porosity (%)	Measured, k_m (m^2)
120	58 ± 5	341	94	0.1	0.0	$(2 \pm 0.6) \times 10^{-15}$
140	81 ± 5	691	233	0.3	0.1	$(6 \pm 0.6) \times 10^{-15}$
160	105 ± 4	1986	885	1.6	0.7	$(2 \pm 0.6) \times 10^{-12}$
180	121 ± 4	6006	5303	6.4	5.7	$(4 \pm 0.7) \times 10^{-12}$
200	173 ± 3	6606	6306	14.4	13.8	$(6 \pm 0.7) \times 10^{-12}$

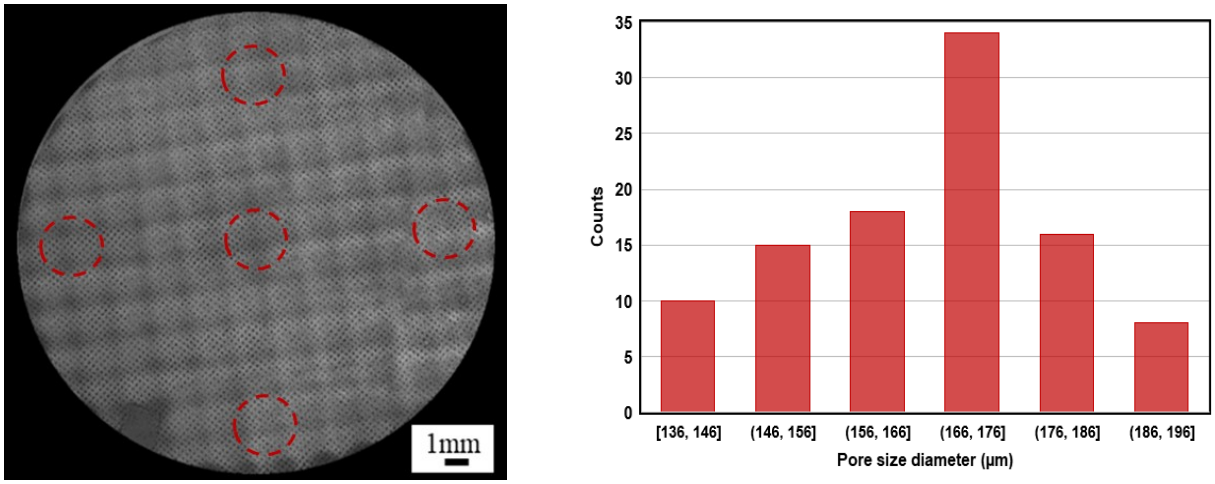

(a) (b)

Figure 4. (a) SEM micrograph of the wavy support with nominal pore size and inter-pore spacing of 200 μm. More than 100 pores from randomly selected locations on the support (e.g. five locations were highlighted) were analysed to determine the openness and size of the pores by using *image J*; (b) resulting pore size distribution of more than 100 randomly selected pores with nominal pore size and inter-pore spacing of 200 μm. Average uncertainty of the pore size is ± 3 μm.

Characterization of membrane support, selective layer and composite membrane

Figures 5a shows an optical micrograph of a 50 mm diameter wavy support with a 37 mm in diameter active area. The morphology of the wavy structure and distribution of the pores can be observed in Figure 5b and 5c, respectively. The surface and cross section of the PES selective layer fabricated by using non-induced phase separation are depicted in Figure 5d-f. The cross-section shows a typical asymmetric membrane structure with a finger-like porous sublayer. The overall thickness of the selective layer was approximately 40 μm with the top dense layer approximately 500 nm. The SEM micrographs along with a topographical image of the wavy 3D composite membrane are reported in Figure 5g-i, showing evidence of conformal adhesion between the selective layer and membrane support, and retention of the underlying wavy structure. Relevant physio-chemical properties of the support, selective layer and the wavy 3D composite membrane are summarized in Table 2. The actual porosity of the composite membrane was 65% and is within the range of commercial microfiltration and ultrafiltration membranes which are typically between 30% and 70 %.[35]

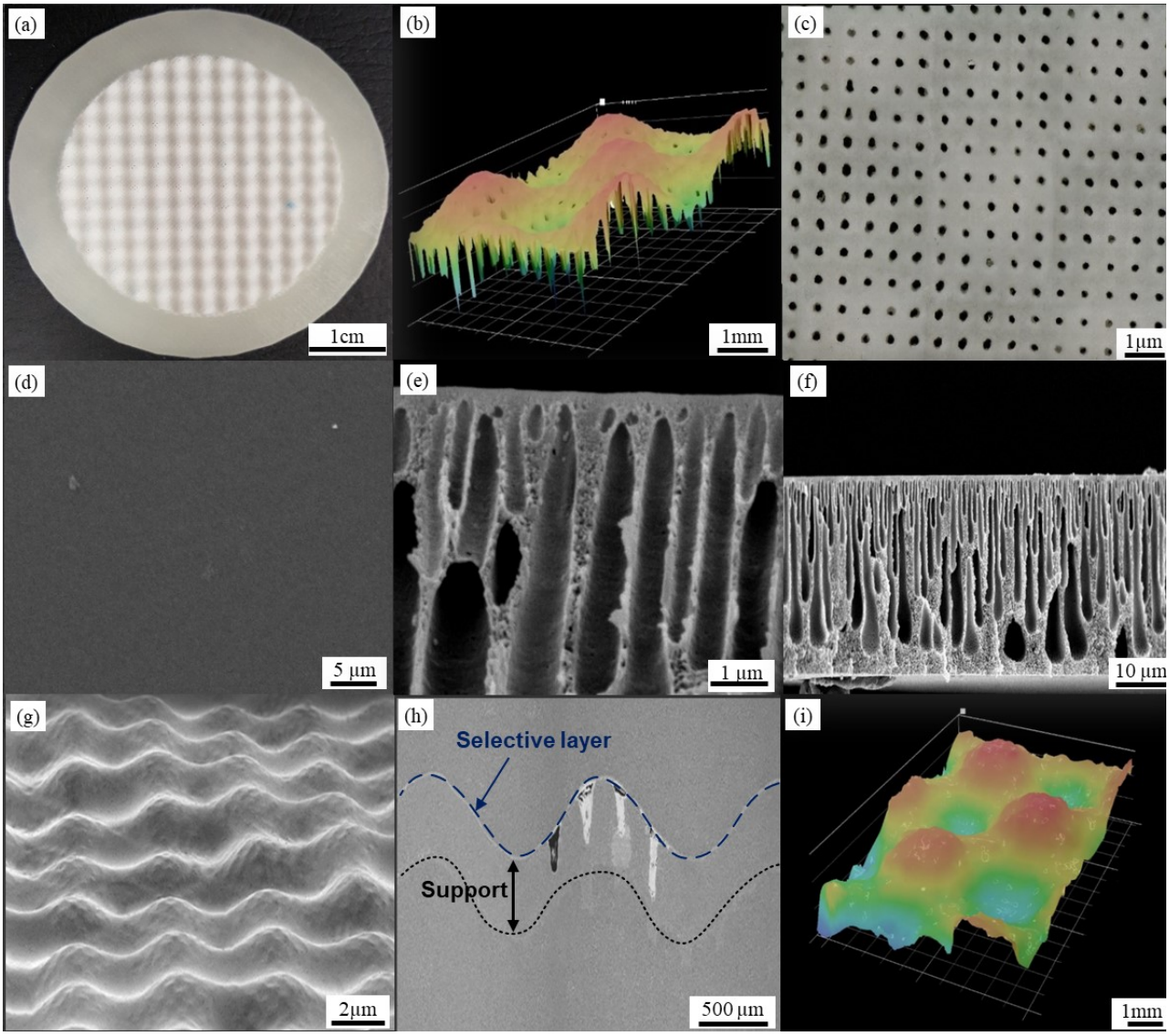

Figure 5. (a) Optical and (b) digital micrographs of 3D printed wavy support. The color map represents the morphology with red indicating the peaks and blue indicating the valleys; (c) SEM micrograph of the 3D wavy support (top view); SEM micrographs of (d) top view and cross section of the PES selective layer at (e) ×10,000 and (f) ×1,000 magnifications; SEM micrographs (g) top view and (h) cross section, and (i) optical micrograph of the wavy composite membrane. The color map represents the morphology with red indicating the peaks and blue indicating the valleys.

Table 2. Physio-chemical properties of the wavy support, selective layer and composite membrane.

	Actual porosity (%)	**MWCO (kDa)**	**Overall thickness (µm)**	***Ra* (nm)**	**k_m (m^2)**	**Contact angle (^{o})**
Membrane support	14 ± 0.6	20000	500 ± 10	73 ± 2	$(6 \pm 0.7) \times 10^{-12}$	83 ± 2
Selective layer	65 ± 2	35 ± 5	40 ± 1	2.9 ± 0.5	$(2 \pm 0.5) \times 10^{-15}$	51 ± 2
Composite membrane	65 ± 2	35 ± 5	540 ± 10	11 ± 1	$(2 \pm 0.7) \times 10^{-15}$	51 ± 2

Filtration performance of 3D printed composite membranes

The permeance profiles of BSA solution (1 g L^{-1}) for flat and wavy 3D composite membranes operated at Re = 1000 and transmembrane pressure (TMP) of 1 bar are shown in Figure 6. Each filtration cycle is comprised of 1 hr of fouling and 15 mins of pure water cleaning. For both membranes, a high BSA rejection (96 ± 1%) was achieved. The initial pure water permeance (PWP) of the wavy composite membrane was approximately 10% higher than for the flat membrane. This is because the wavy structure had an effective filtration area of approximately 13% higher than the flat one for the same footprint (50 mm).[26] This is one of the advantages of fabricating patterned membranes by 3D printing since for other techniques, such as nanoimprinting, which impinge on the membrane's surface, resulting in a reduction in either the size and/or the number of pores.[17]

A marked permeance decline (~61%) was observed for the flat composite membrane upon the start of the BSA filtration due to concentration polarization and fouling,[36] and immediately reached a steady-state value. A significantly lower reduction (~38%) was observed for the wavy 3D composite membrane. This strongly suggests that lower concentration polarization and rate of BSA deposition[37] were achieved compared to the flat membrane. Following the BSA filtration, a minimal recovery in PWP was observed for the as-fouled flat membrane after flushing of the system with water. On the other hand, the PWP of the wavy membrane increased significantly, indicating that more loosely attached BSA could be washed away from the surface of the wavy membrane. The wavy membrane retained ~85% of its initial permeance after three filtration cycles, whereas the flat

membrane could only retain ~36% of the initial permeance. These observations revealed that the presence of the wavy structure significantly reduced BSA deposition over the membranes' surface making rinsing with water alone (i.e. without added chemicals) much more effective. This is attributed to the improved hydrodynamics i.e. higher surface stress and primary recirculation for the wavy 3D composite membrane, as observed for other patterned (nano-imprinted patterns[38], soft-lithographic prisms[39], and moulding of pyramids[32]) membranes. The permeance profile of BSA solution for flat and wavy membranes operated under Re = 400 and 800 both at TMP of 1 bar were also performed and the results shown in Figure S3. Similar filtration behaviours were observed, with the wavy 3D composite membranes out-performing the flat ones.

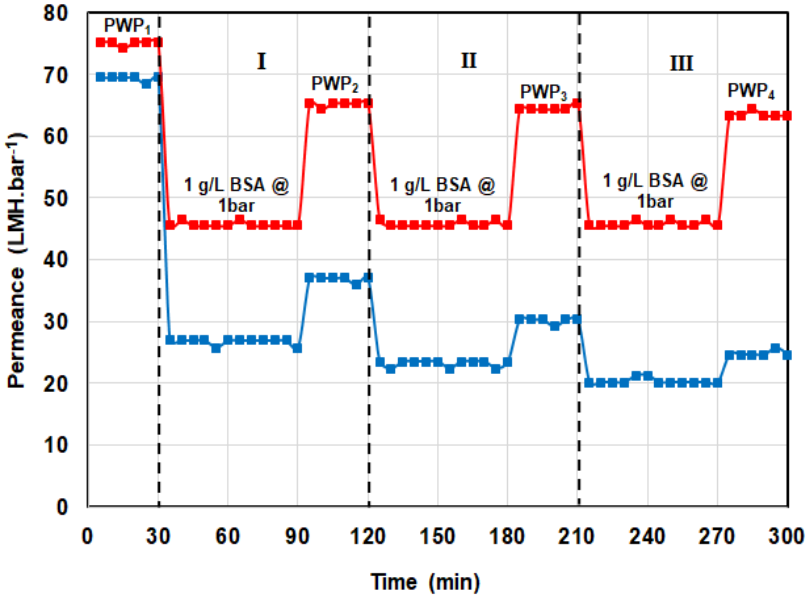

Figure 6. Permeance profiles of BSA solution (1 g L^{-1}) for flat (blue) and wavy (red) membranes during 3 filtration cycles (1 hr of fouling and 15 min of pure water cleaning per cycle) operated at Re = 1000 and TMP = 1 bar. Regions identified by roman numerals represent the 3 filtration cycles. Average uncertainty of the permeance is ± 0.4 LMH bar^{-1}.

Quantitative comparison of the filtration performance could also be expressed in terms of the permeance recovery ratio (PRR) and total permeance decline ratio (PDR). Figure 7 shows the PRR and PDR for both the flat and wavy 3D composite membranes for Re = 400, 800 and 1000. It is clear that the values of PRR for the wavy membrane are consistently higher than the flat membranes', a

desired feature for an effective procedure for BSA removal. Similarly, the values of PDR for wavy membranes for all Re were consistently lower than the flat one, making it easier to remove any accumulated fouling. As expected, PRR increases with Re since the surface shear stress imposed on the BSA fouling layer also increases. A summary of PRR, PDR, reversible permeance decline ratio (RPR), irreversible permeance decline ratio (IrPR) values for flat and wavy 3D composite membranes as a function of Re number can be found in Table S3.

The nature of BSA fouling could be characterized by the reversible permeance decline ratio (RPR) and the irreversible permeance decline ratio (IrPR). The former is associated with BSA fouling that is reversible upon front washing with water without any kind of mechanical or chemical cleaning, whereas the latter is the permanent fouling caused by BSA entering and depositing in the membrane pores. The sum of RPR and IrPR gives the PDR. It is clear from Table S3 that the proportion of irreversible fouling for the wavy composite membrane is consistently lower than the flat membrane for all the Re values tested. This is a desirable feature because it suggests that the largest portion of reversible fouling of the wavy composite membrane could be removed by simply front washing with water. The effect becomes more significant for Re = 1000.

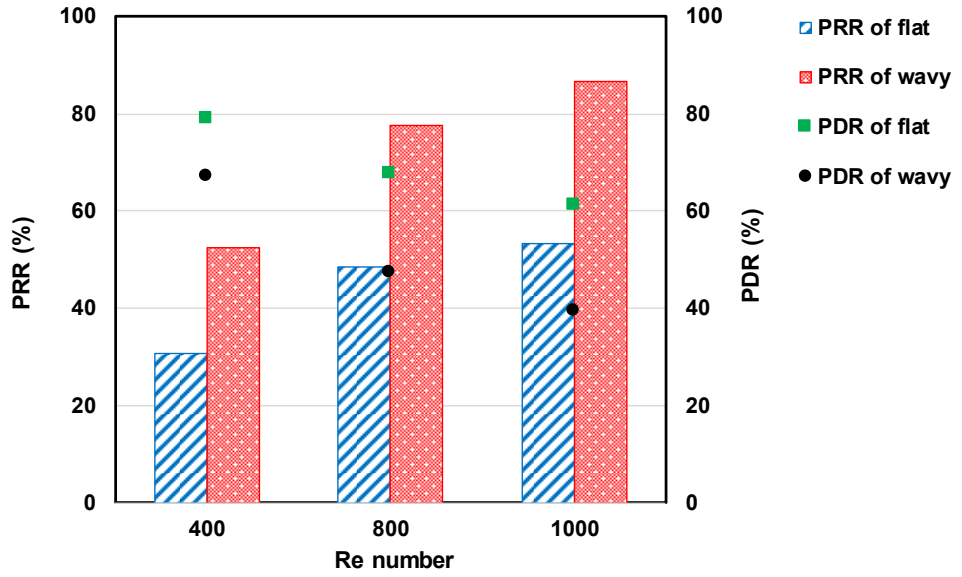

Figure 7. The PRR and PDR of flat and wavy 3D composite membranes after the first filtration cycle as a function of Reynolds number. Average uncertainty of the PRR and PDR is ± 0.9 %.

A series of particle tracing CFD simulations were performed to further elucidate the fouling behaviour of BSA on the flat (Figure 8a) and wavy membranes (Figure 8b). Details of model development are provided in the supporting information. In the model, BSA particles introduced at the inlet (left boundary) could either attach to the membrane surface (bottom boundary) or exit through the outlet (right boundary). The BSA particles enter the valley regions of the wavy structure due to the permeation drag but can escape this region and return to the bulk cross-flow stream only when primary recirculation, induced by the wavy pattern, is present (Figure 3). The CFD simulations supports the results observed in the experiments shown in Figures 6 and 7.

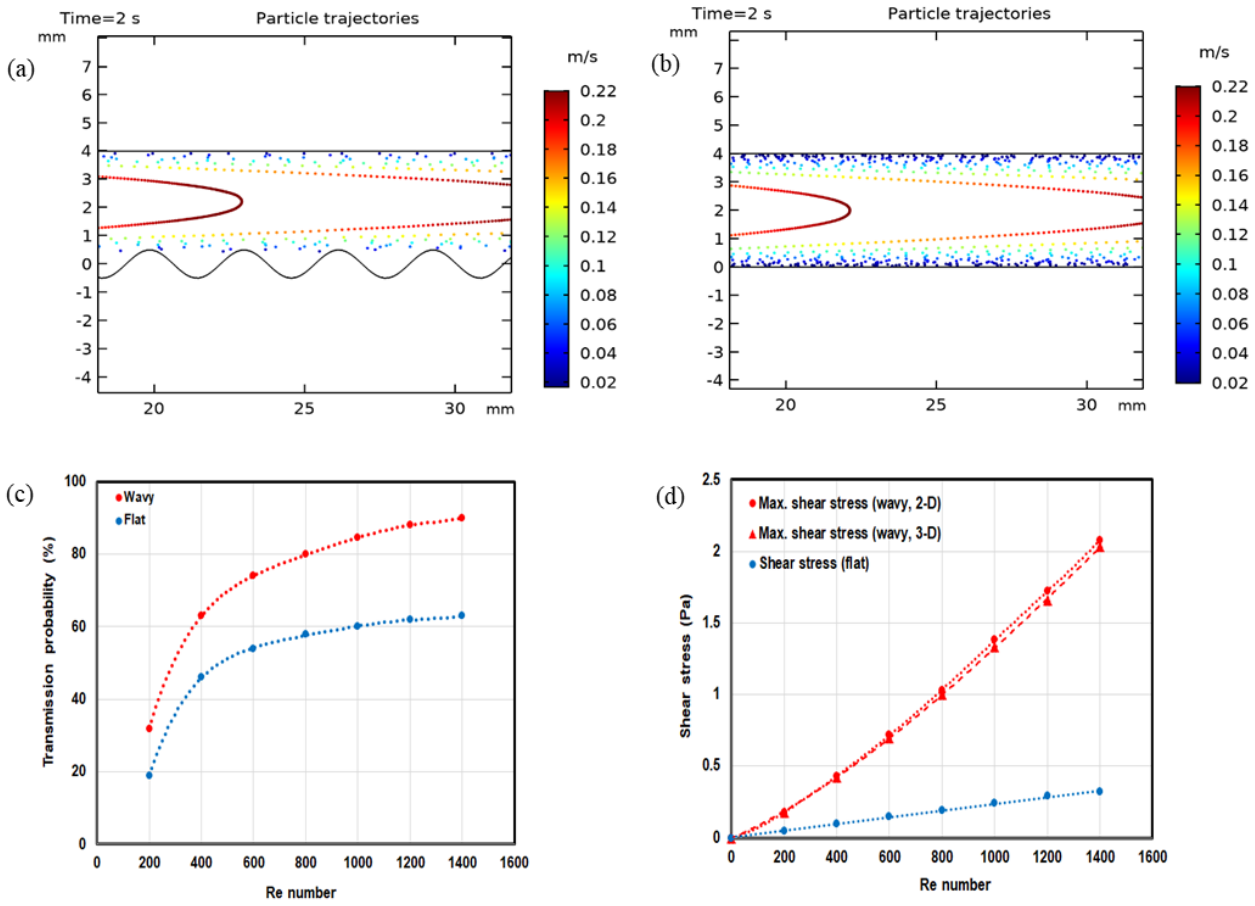

Figure 8. Particle trajectories for (a) wavy and (b) flat 3D composite membranes at Re = 1000; (c) Transmission probability (TP) values for at different Re numbers; and (d) Maximum surface shear stress values as a function of Re number.

CFD can also provide a measure of the extent of fouling using the transmission probability (TP) parameter, which is calculated by dividing the total number of particles passing the outlet by the number of particles introduced at the inlet. Figure 8c shows that the amount of BSA particles exiting the outlet for the wavy membrane is higher than for the flat membrane, indicating less fouling. This observation is strongly linked to the increase in surface shear stress imposed on the wavy membrane (Figure 8d). The maximum surface shear stress for the wavy pattern was significantly higher than the one for the flat membrane under all Re numbers tested, providing a clear explanation as to why the particles tend not to stick onto the surface of the wavy membrane. With increasing Re numbers, the difference in the maximum surface shear stress between the wavy and flat membranes increases, with the former reaching 1.43 Pa compared to 0.26 Pa of the latter for Re = 1000. Interestingly, the shear stress value generated from the wavy membrane are in the same order of magnitude with those employed in cleaning-in-place processes in the dairy industry.[33] The velocity profiles and particle trajectories for Re = 400 and Re = 800 are presented in Figure S4.

Long-term filtration performance of wavy composite membrane

Ten (10) BSA filtration cycles (30 mins of fouling and 15 mins of pure water cleaning per cycle) at Re = 1000 were carried out to further test the filtration performance of the wavy membranes. For a membrane to be of practical use, the fouling-resistant behaviour has to last at least the length of time between two cleaning cycles[7], thereby decreasing operational costs. Figure 9 shows that a good level of PWP could be maintained after 10 cycles. Apart from the first cycle, the value of PRR could maintained at approximately 98 %. In fact, the water permeance decreased only 13%, from 75 to 65 $LMH.bar^{-1}$, after 10 complete cycles of BSA filtration and flushing with water alone.

This enhanced fouling-resistant behaviour can be attributed to the turbulence generated near the surface by the wavy structure, as discussed earlier, proving that hydrodynamics can prolong the time interval between aggressive chemical cleaning. In turn, this promises to extend the useful life of

these membranes and, hence, reduce operational and environmental costs of membrane processes. The values of PRR, RPR, IrPR and PDR for each cycle are reported in Table S4.

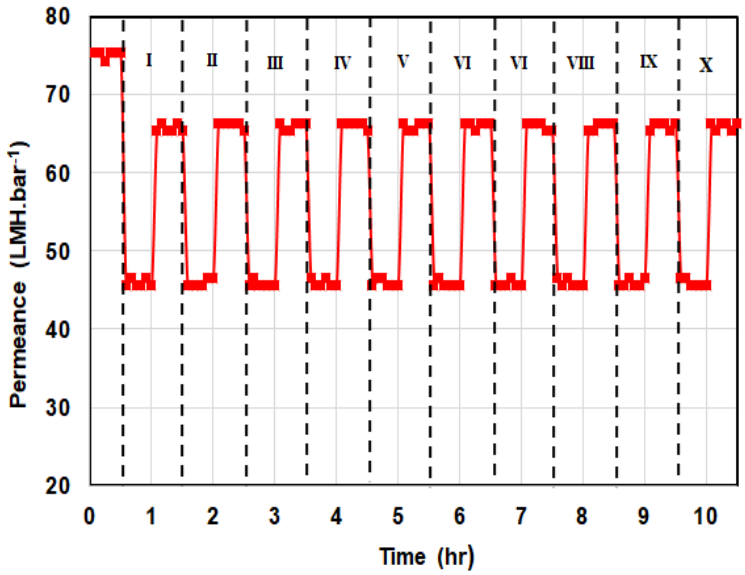

Figure 9. Permeance profile of BSA solution (1 g L^{-1}) with wavy 3D composite membrane during 10 filtration cycles (30 min of fouling and 15 min of cleaning per cycle) at Re = 1000, using only pure water flushing between each cycle. Regions identified by roman numerals represent the 10 filtration cycles. Average uncertainty is ± 0.4 LMH bar^{-1}.

The scale-up or -down of filtration process is rarely linear, and therefore not straight-forward. For instance, the size of flow recirculations and shear stress generated by the wavy surface will not scale linearly with waviness of the membrane or feed flow rates even when geometric and dynamic similarities are maintained. Nevertheless, the series of computational model developed in this work could be easily modified to provide insights to the hydrodynamics (i.e. shear stress, flow patterns and particle tracing) of scaled-up or -down filtration systems. The models could also be flexibly applied to other membrane geometries. This will enable one to make informed decisions about the optimum membrane configurations and operating conditions. The computing capacity and time required to process and 3D print industrial scale and more complex membrane geometry remains a challenge. The authors, however, are confident that this limitation will progressively become less significant as computing and 3D printing technology continue to develop.

CONCLUSIONS

This paper demonstrates the success of fabrication of fouling-resistant ultrafiltration composite membranes where the patterned membrane support was 3D printed and the thin PES selective layer was prepared by using non-induced phase separation. The power of combining CFD modelling and material characterisation to identify the ideal set of membrane design parameters and operating conditions for a specific application has been revealed. CFD with particle tracing has also been used as a quantitative tool to provide valuable information on the fluid mechanics of the filtration process. The optical and electron micrographs of the 3D supports showed that UV-cured polyurethane acrylate oligomers are promising materials for membrane supports with controlled morphology and surface roughness. These characteristics were crucial for the strong adhesion of the thin PES selective layer.

Filtration experiments of BSA revealed that the wavy 3D composite membrane exhibited superior fouling-resistant performance compared to flat membranes for multiple (1, 3 and 10 cycles) filtration cycles under all the operating conditions (TMP = 1 bar and Re = 400, 800 and 1000) employed in this study. The ability of the optimised wavy 3D composite membrane to retain 88% of its initial permeance after 10 complete cycles, using only water as cleaning agent, was striking. These results show that a suitable chemical-free approach to mitigate fouling for extended membrane operations can be achieved by using carefully designed 3D printed composite membranes.

ASSOCIATED CONTENT

Supporting Information: Governing equations and boundary conditions used in the numerical simulations; Schematic of the cross-flow filtration setup; Summary of relevant fouling and cleaning studies of patterned membranes; Images of membrane supports after chemical compatibility test and intrinsic permeability of wavy membrane supports; Permeance profiles of BSA solution for flat and wavy composite membranes; The PRR, RPR, IrPR and PDR values (%) of flat and wavy membranes; Flow patterns and velocity vectors of BSA solution for wavy composite membrane; The PRR, RPR, IrPR and PDR values (%) of wavy composite membrane for 10 filtration cycles.

ACKNOWLEDGEMENTS

This work is supported by the Engineering and Physical Sciences Research Council (EPSRC) UK (Grant EP/M01486X/1). The authors are grateful to Dr Darrell Patterson, for fruitful discussions and Keyence UK Ltd, for taking the image which is shown in Figures 5b and 5i.

AUTHOR INFORMATION

Corresponding author: *Email: y.m.chew@bath.ac.uk

ORCID: Y.M. John Chew: 0000-0003-2888-834X

Author contributions: Y.M.J.C. and D.M. designed the project. A.A. and S.M. conducted the experiments. Y.M.J.C. and S.M. performed the numerical simulations. A.A., Y.M.J.C., D.M. and S.M. analysed all the experimental and simulation data. The manuscript was written with contributions from all authors. All authors have approved the final version of the manuscript.

ABBREVIATIONS

ABS, Acrylonitrile butadiene styrene

AFM, Atomic force microscopy

BSA, Bovine serum albumin

CAD, Computer-aided drafting

CFD, Computational fluid dynamics

DI, Deionized water

DMAc, Dimethylacetamide

DMF, Dimethylformamide

DMSO, Dimethyl sulfoxide

IrPR, Irreversible permeance decline ratio

MJP, Multi-jet printing

MWCO, Molecular weight cut-off

NIPS, Non-induced phase separation

NMP, N-Methyl-2-pyrrolidone

PBS, Phosphate buffer saline

PDR, Total permeance decline ratio

PES, Polyethersulfone

PEG, Polyethylene glycol

PRR, Permeance recovery ratio

PTFE, Polytetrafluoroethylene

PVDF, Polyvinylidene fluoride

PWP, Pure water permeance

RPR, Reversible permeance decline ratio

STL, Stereolithography

TMP, Transmembrane pressure

TP, Transmission probability

UF, Ultrafiltration

REFERENCES

(1) Goosen, M.; Sablani, S.; Al-Hinai, H.; Al-Obeidani, S.; Al-Belushi, R.; Jackson, a. Fouling of Reverse Osmosis and Ultrafiltration Membranes: A Critical Review. *Separation Science and Technology* **2005,** *39*, 2261-2297.

(2) Gao, W.; Liang, H.; Ma, J.; Han, M.; Chen, Z.-l.; Han, Z.-s.; Li, G.-b. Membrane Fouling Control in Ultrafiltration Technology for Drinking Water Production: A Review. *Desalination* **2011,** *272*, 1-8.

(3) Chew, C. M.; Aroua, M.; Hussain, M.; Ismail, W. W. Practical Performance Analysis of an Industrial-scale Ultrafiltration Membrane Water Treatment Plant. *Journal of the Taiwan Institute of Chemical Engineers* **2015,** *46*, 132-139.

(4) Shi, X.; Tal, G.; Hankins, N. P.; Gitis, V. Fouling and Cleaning of Ultrafiltration Membranes: A Review. *Journal of Water Process Engineering* **2014,** *1*, 121-138.

(5) Vrijenhoek, E. M.; Hong, S.; Elimelech, M. Influence of Membrane Surface Properties on Initial Rate of Colloidal Fouling of Reverse Osmosis and Nanofiltration Membranes. *Journal of Membrane Science* **2001,** *188*, 115-128.

(6) Ma, H.; Bowman, C. N.; Davis, R. H. Membrane Fouling Reduction by Backpulsing and Surface Modification. *Journal of Membrane Science* **2000,** *173*, 191-200.

(7) Porcelli, N.; Judd, S. Chemical Cleaning of Potable Water Membranes: A Review. *Separation and Purification Technology* **2010,** *71*, 137-143.

(8) Vogelaar, L.; Barsema, J. N.; van Rijn, C. J. M.; Nijdam, W.; Wessling, M. Phase Separation Micromolding-PSμM. *Advanced Materials* **2003,** *15*, 1385-1389.

(9) Heinz, O.; Aghajani, M.; Greenberg, A. R.; Ding, Y. Surface-patterning of Polymeric Membranes: Fabrication and Performance. *Current opinion in chemical engineering* **2018,** *20*, 1-12.

(10) Won, Y.-J.; Lee, J.; Choi, D.-C.; Chae, H. R.; Kim, I.; Lee, C.-H.; Kim, I.-C. Preparation and Application of Patterned Membranes for Wastewater Treatment. *Environmental Science & Technology* **2012,** *46*, 11021-11027.

(11) Won, Y.-J.; Choi, D.-C.; Jang, J. H.; Lee, J.-W.; Chae, H. R.; Kim, I.; Ahn, K. H.; Lee, C.-H.; Kim, I.-C. Factors Affecting Pattern Fidelity and Performance of a Patterned Membrane. *Journal of Membrane Science* **2014,** *462*, 1-8.

(12) Maruf, S. H.; Rickman, M.; Wang, L.; Mersch IV, J.; Greenberg, A. R.; Pellegrino, J.; Ding, Y. Influence of Sub-micron Surface Patterns on the Deposition of Model Proteins During Active Filtration. *Journal of Membrane Science* **2013,** *444*, 420-428.

(13) Xie, M.; Luo, W.; Gray, S. R. Surface Pattern by Nanoimprint for Membrane Fouling Mitigation: Design, Performance and Mechanisms. *Water Research* **2017,** *124*, 238-243.

(14) Kharraz, J. A.; Bilad, M.; Arafat, H. A. Simple and Effective Corrugation of PVDF Membranes for Enhanced MBR Performance. *Journal of Membrane Science* **2015,** *475*, 91-100.

(15) Kharraz, J. A.; Bilad, M.; Arafat, H. A. Flux Stabilization in Membrane Distillation Desalination of Seawater and Brine Using Corrugated PVDF Membranes. *Journal of Membrane Science* **2015,** *495*, 404-414.

(16) Nawi, M.; Izati, N.; Bilad, M. R.; Zolkhiflee, N.; Nordin, N. A. H.; Lau, W. J.; Narkkun, T.; Faungnawakij, K.; Arahman, N.; Mahlia, T. M. I. Development of A Novel Corrugated Polyvinylidene difluoride Membrane via Improved Imprinting Technique for Membrane Distillation. *Polymers* **2019,** *11*, 865.

(17) Maruf, S. H.; Greenberg, A. R.; Pellegrino, J.; Ding, Y. Critical Flux of Surface-Patterned Ultrafiltration Membranes During Cross-flow Filtration of Colloidal Particles. *Journal of Membrane Science* **2014,** *471*, 65-71.

(18) Low, Z.-X.; Chua, Y. T.; Ray, B. M.; Mattia, D.; Metcalfe, I. S.; Patterson, D. A. Perspective on 3D Printing of Separation Membranes and Comparison to Related Unconventional Fabrication Techniques. *Journal of Membrane Science* **2017,** *523*, 596-613.

(19) Wang, X.; Jiang, M.; Zhou, Z.; Gou, J.; Hui, D. 3D Printing of Polymer Matrix Composites: A Review and Prospective. *Composites Part B: Engineering* **2017,** *110*, 442-458.

(20) Ngo, T. D.; Kashani, A.; Imbalzano, G.; Nguyen, K. T.; Hui, D. Additive Manufacturing (3D printing): A Review of Materials, Methods, Applications and Challenges. *Composites Part B: Engineering* **2018,** *143*, 172-196.

(21) Melchels, F.P.W.; Feijen, J.,; Grijpma, D.W. A Review on Stereolithography and Its Application in Biomedical Engineering. *Biomaterials* **2010,** 31, 6121-6130.

(22) Seo, J.; Kushner, D. I.; Hickner, M. A. 3D Printing of Micropatterned Anion Exchange Membranes. *ACS Applied Materials & Interfaces* **2016,** *8*, 16656-16663.

(23) Femmer, T.; Kuehne, A. J. C.; Torres-Rendon, J.; Walther, A.; Wessling, M. Print Your Membrane: Rapid Prototyping of Complex 3D-PDMS Membranes via a Sacrificial Resist. *Journal of Membrane Science* **2015,** *478*, 12-18.

(24) Wardrip, N. C.; Dsouza, M.; Urgun-Demirtas, M.; Snyder, S. W.; Gilbert, J. A.; Arnusch, C. J. Printing-Assisted Surface Modifications of Patterned Ultrafiltration Membranes. *ACS Applied Materials & Interfaces* **2016,** *8*, 30271-30280.

(25) Badalov, S.; Oren, Y.; Arnusch, C. J. Ink-jet Printing Assisted Fabrication of Patterned Thin Film Composite Membranes. *Journal of Membrane Science* **2015,** *493*, 508-514.

(26) Al-Shimmery, A.; Mazinani, S.; Ji, J.; Chew, Y. M. J.; Mattia, D. 3D Printed Composite Membranes With Enhanced Anti-fouling Behaviour. *Journal of Membrane Science* **2019,** *574*, 76-85.

(27) Chew, Y. J.; Paterson, W.; Wilson, D. Fluid Dynamic Gauging: A New Tool to Study Deposition on Porous Surfaces. *Journal of Membrane Science* **2007,** *296*, 29-41.

(28) Evenepoel, N.; Wen, S.; Tilahun Tsehaye, M.; Van der Bruggen, B. Potential of DMSO as Greener Solvent for PES Ultra- and Nanofiltration Membrane Preparation. *Journal of Applied Polymer Science* **2018,** *135*, 46494.

(29) Lewis, W. J. T.; Agg, A.; Clarke, A.; Mattsson, T.; Chew, Y. M. J.; Bird, M. R. Development of An Automated, Advanced Fluid Dynamic Gauge for Cake Fouling Studies in Cross-flow Filtrations. *Sensor Actuat a-Phys* **2016,** *238*, 282-296.

(30) Zhang, J.; Xu, Z.; Mai, W.; Min, C.; Zhou, B.; Shan, M.; Li, Y.; Yang, C.; Wang, Z.; Qian, X. Improved Hydrophilicity, Permeability, Antifouling and Mechanical Performance of PVDF Composite Ultrafiltration Membranes Tailored by Oxidized Low-dimensional Carbon Nanomaterials. *Journal of Materials Chemistry A* **2013,** *1*, 3101-3111.

(31) Xu, L.; Shahid, S.; Shen, J.; Emanuelsson, E. A. C.; Patterson, D. A. A Wide Range and High Resolution One-filtration Molecular Weight Cut-off Method for Aqueous Based Nanofiltration and Ultrafiltration membranes. *Journal of Membrane Science* **2017,** *525*, 304-311.

(32) Lee, Y. K.; Won, Y.-J.; Yoo, J. H.; Ahn, K. H.; Lee, C.-H. Flow Analysis and Fouling on the Patterned Membrane Surface. *Journal of Membrane Science* **2013,** *427*, 320-325.

(33) Chew, J.; Paterson, W.; Wilson, D. Fluid Dynamic Gauging for Measuring the Strength of Soft Deposits. *Journal of Food Engineering* **2004,** *65*, 175-187.

(34) Chua, C. K.; Leong, K. F. *3D Printing and Additive Manufacturing: Principles and Applications (with Companion Media Pack) of Rapid Prototyping Fourth Edition*, World Scientific Publishing Company: 2014.

(35) Baker, R. W. *Membrane technology and applications*, John Wiley & Sons: 2012.

(36) Van den Berg, G.; Smolders, C. Flux Decline in Ultrafiltration Processes. *Desalination* **1990,** *77*, 101-133.

(37) Jones, K. L.; O'Melia, C. R. Protein and Humic Acid Adsorption onto Hydrophilic Membrane Surfaces: Effects of pH and Ionic Strength. *Journal of Membrane Science* **2000,** *165*, 31-46.

(38) Maruf, S. H.; Wang, L.; Greenberg, A. R.; Pellegrino, J.; Ding, Y. Use of Nanoimprinted Surface Patterns to Mitigate Colloidal Deposition on Ultrafiltration Membranes. *Journal of Membrane Science* **2013,** *428* (Supplement C), 598-607.

(39) Won, Y.-J.; Jung, S.-Y.; Jang, J.-H.; Lee, J.-W.; Chae, H.-R.; Choi, D.-C.; Hyun Ahn, K.; Lee, C.-H.; Park, P.-K. Correlation of Membrane Fouling with Topography of Patterned Membranes for Water Treatment. *Journal of Membrane Science* **2016,** *498*, 14-19.